INTERNATIONAL ATOMIC ENERGY AGENCY
UNITED NATIONS EDUCATIONAL, SCIENTIFIC AND CULTURAL ORGANIZATION
INTERNATIONAL CENTRE FOR THEORETICAL PHYSICS
I.C.T.P., P.O. BOX 586, 34100 TRIESTE, ITALY, CABLE: CENTRATOM TRIESTE

UNITED NATIONS INDUSTRIAL DEVELOPMENT ORGANIZATION

INTERNATIONAL CENTRE FOR SCIENCE AND HIGH TECHNOLOGY
c/o INTERNATIONAL CENTRE FOR THEORETICAL PHYSICS 34100 TRIESTE (ITALY) VIA GRIGNANO 9 ADRIATICO PALACE P.O. BOX 586 TELEPHONE 040-224572 TELEFAX 040-224575 TELEX 460449 APH I

SMR/760-23

"College on Atmospheric Boundary Layer and Air Pollution Modelling"
16 May - 3 June 1994

"Lagrangian Particle Dispersion Modeling in Mesoscale Applications"

M. ULIASZ
Department of Atmospheric Sciences
Colorado State University
Fort Collins, CO
USA

Please note: These notes are intended for internal distribution only.

to appear in Environmental Modeling II (ed. P. Zannetti)

Chapter

Lagrangian particle dispersion modeling in mesoscale applications

Marek Uliasz

Department of Atmospheric Sciences, Colorado State University
Fort Collins, CO 80523, U.S.A.
(also at Warsaw University of Technology, Poland)

Abstract

This chapter presents some experiences resulting from development and applications of two dispersion modeling systems based on the Lagrangian particle modeling: (1) Mesoscale Dispersion Modeling System (MDMS), and (2) Hybrid Particle Concentration Transport (HYPACT) model. A special attention is paid to the development of an efficient modeling tool to perform intensive calculations of air pollution dispersion on mesoscale and regional scales. These efforts go in several directions: (1) evaluation of simplifications of the Lagrangian particle models acceptable in mesoscale applications; (2) combining different modeling techniques in hybrid dispersion models; (3) using an alternative receptor-oriented approach in dispersion modeling. Methods for concentration calculations and physical parameterizations in the particle models are also shortly reviewed. Two examples of applications of the Lagrangian particle dispersion model for complex terrain in the southwestern United States and eastern Europe demonstrate a design of computationally intensive air quality studies with the aid of the modern workstations.

Keywords

air pollution modeling, Lagrangian particle models, mesoscale models, receptor modeling

1 Introduction

Lagrangian particle models have recently become a very important tool for studying air pollution dispersion (e.g., Zannetti, 1992). They are based on assumption that

atmospheric diffusion can be modelled by a Markov chain process first proposed by Obukhov (Obukhov, 1959) and Smith (Smith, 1968). Although the concept of particle dispersion modeling is not new, its widespread application has been limited by (1) a lack of available 3-D meteorological input data and (2) considerable computational requirements. It was especially true in the case of mesoscale dispersion of pollutants in the 20 to 2000 km range where influence of the landscape variability and complex terrain on atmospheric transport must be taken into account. Recent advances in computer technology make it possible to link Lagrangian particle dispersion models to numerical mesoscale meteorological models suitable to simulate atmospheric circulations in complex terrain (Pielke et al., 1991; Lyons et al., 1993). A real revolution in mesoscale dispersion applications has been introduced by powerful and affordable workstations (Grubb and Borchers, 1991) which can be dedicated to specific tasks. The workstations allow us to fully utilize visualization capabilities of the particle modeling technique.

This chapter presents some experiences resulting from development and applications of two dispersion modeling systems based on the Lagrangian particle modeling:

- Mesoscale Dispersion Modeling System (MDMS)
- Hybrid Particle Concentration Transport (HYPACT) model

The MDMS was originally developed on a personal computer in Warsaw University of Technology, Poland (Uliasz, 1990a; Uliasz, 1990b; Uliasz, 1993) and then used in different applications on Unix workstations at Colorado State University (CSU). This system includes a 3-D hydrostatic meteorological mesoscale model (MESO), a Lagrangian Particle Dispersion (LPD) model and an Eulerian Grid Dispersion (EGD) model. The LPD model is used not only with the MESO model but also with other meteorological models including the CSU Regional Atmospheric Modeling System (RAMS) (Pielke et al., 1992). The HYPACT is a new dispersion code being developed at ASTER, Inc.. It is designed to be used with the newest version of the CSU RAMS and includes more advanced physical parameterizations in the particle dispersion model as well as the concept of a hybrid Lagrangian-Eulerian dispersion modeling.

Despite of advances in computer technology, the particle models are still computationally expensive if it is necessary to track a large number of particles for long distances and for a long time. This problem appears in mesoscale applications, especially, when multiple pollution sources with continuous emissions are considered. The goal of the presented research is the development of an efficient modeling tool to perform intensive calculations of air pollution dispersion on mesoscale and regional scales. These efforts go in several directions: (1) evaluation of simplifications of the Lagrangian particle models acceptable in mesoscale applications; (2) combining different modeling techniques in hybrid dispersion models; (3) using an alternative receptor-oriented approach in dispersion modeling. Our experiences in concentration calculations and physical parameterizations in the particle models are also shortly reviewed. Finally, two examples of applications of the LPD model for complex terrain in

the southwestern United States and eastern Europe demonstrate a design of computationally intensive air quality studies with the aid of the modern workstations. These projects emphasize the application of the receptor-oriented dispersion modeling.

2 Model equations

Pollution dispersion in the LPD model is simulated by tracking a large set of particles. Subsequent positions of each particle, representing a discrete element of pollutant mass, are computed from the following relations

$$X(t+\Delta t) = X(t) + (u+u')\Delta t \quad (1)$$
$$Y(t+\Delta t) = Y(t) + (v+v')\Delta t \quad (2)$$
$$Z(t+\Delta t) = Z(t) + (w+w'+w_p)\Delta t \quad (3)$$

The resolvable scale components of wind velocity u, v and w are obtained directly from the meteorological model. Three Markov chain schemes (LPD2a, LPD2b, LPD2c) and two fully random walking schemes (LPD1b, LPD1c) are considered to create the turbulent wind components u', v', and w' (Uliasz and Pielke, 1993). The most advanced model, LPD2a, is used as a reference and all other model versions are obtained by its subsequent simplifications. In addition, an option without turbulent diffusion (LPD0) where particles are moved explicitly by the resolved wind can be used to calculate trajectories and streaklines. An additional vertical velocity component, w_p, in (3) takes into account gravitational settlement of heavy particles and buoyancy phenomena.

Model LPD2a. The Markov process including wind velocity covariances is defined by the scheme proposed by Zannetti (1986):

$$u'(t) = \phi_1 u'(t-\Delta t) + \sigma_{ru}\eta_u \quad (4)$$
$$v'(t) = \phi_2 v'(t-\Delta t) + \phi_3 u'(t) + \sigma_{rv}\eta_v \quad (5)$$
$$w'(t) = \phi_4 w'(t-\Delta t) + \phi_5 v'(t) + \phi_6 u'(t) + (\sigma_{rw}\eta_w + w_d) \quad (6)$$

The coefficients $\phi_1,\ldots,\phi_6$ are expressed by the wind velocity variances, σ_u^2, σ_v^2, σ_w^2, covariances, $\overline{u'w'}$, $\overline{v'w'}$, $\overline{u'v'}$, and Lagrangian autocorrelations R_u, R_v, R_w. The last terms are random normally-distributed components; η_u, η_v, and η_w are random numbers from a standard Gaussian distribution. The random component of vertical velocity has a nonzero mean value w_d, called a drift velocity, to prevent the spurious accumulation of particles in regions of low turbulence (Legg and Raupach, 1982). The Lagrangian velocity autocorrelations are expressed by Lagrangian time scales, e.g., $R_w(\Delta t) = \exp(-\Delta t/T_{Lw})$.

The time step Δt used to move particles in the Markov chain model versions is variable in inhomogeneous turbulence and depends on the Lagrangian time scale, T_{Lw}: $\Delta t = max\,(0.1T_{Lw},\ \Delta t_{min})$. The minimum time step Δt_{min} is arbitrary prescribed to avoid a zero time step near the ground surface.

Model LPD2b. If the covariances of wind velocity components are neglected, the model LPD2a is simplified to the form:

$$u'(t) = R_u u'(t-\Delta t) + (1-R_u^2)\sigma_u\eta_u \quad (7)$$
$$v'(t) = R_v v'(t-\Delta t) + (1-R_v^2)\sigma_v\eta_v \quad (8)$$
$$w'(t) = R_w w'(t-\Delta t) + (1-R_w^2)\sigma_w\eta_w + w_d \quad (9)$$

This model version can be further simplified to the model LPD2c by neglecting the horizontal turbulent wind components:

$$u'(t) = 0 \quad (10)$$
$$v'(t) = 0 \quad (11)$$
$$w'(t) = R_w w'(t-\Delta t) + (1-R_w^2)\sigma_w\eta_w + w_d \quad (12)$$

Model LPD1b. This model version is obtained from the model LPD2b by increasing the time step Δt used to move particles. Assuming that Δt is much larger than the Lagrangian time scales, the scheme is derived where particles have no memory and move fully randomly at each time step:

$$u'(t) = \sigma_u\eta_u \quad (13)$$
$$v'(t) = \sigma_v\eta_v \quad (14)$$
$$w'(t) = \sigma_w\eta_w + w_d \quad (15)$$

The time step Δt is kept constant (typically Δt = 180 s). After neglecting the horizontal turbulent velocity components in the above equations the simplest variant, model LPD1c, is obtained. The random walk model versions do not require the knowledge of Lagrangian time scales.

The wind velocity variances and covariances required by the LPD model are calculated diagnostically from available meteorological information using a simplified second-order closure technique developed by Mellor and Yamada (Mellor and Yamada, 1982; Helfand and Labraga, 1988; Andrén, 1990). A so-called level 2.5 scheme modified for a case of growing turbulence (Helfand and Labraga, 1988) is applied if the fields of wind, potential temperature, and turbulent kinetic energy are provided by the meteorological model which uses the same turbulence parameterization. This scheme is based on the prognostic equation for the turbulent kinetic energy solved in the meteorological model. A simpler level 2.0 scheme is used if only wind and potential temperature fields are available from the meteorological model or observations. This scheme assumes an exact balance between production of turbulent energy and dissipation. The Lagrangian time scales are calculated from turbulent length scale, l, and wind velocity variances

$$T_{Lu} = c_T l/\sigma_u, \quad T_{Lv} = c_T l/\sigma_v, \quad T_{Lw} = c_T l/\sigma_w \quad (16)$$

The constant c_T is assumed to be 1 which provides a good agreement between the Lagrangian time scale, T_{Lw}, simulated in the model and given by empirical formulae for

an idealized case of a horizontally homogeneous atmospheric boundary layer (Hanna, 1982). Equations (16) indicate that the Markov chain particle models may be quite sensitive to the turbulent length scale, l. Formulation of a proper turbulent length scale in mesoscale meteorological models applied for complex terrain simulations still requires further research. It should be also pointed out that the Lagrangian time scale, T_{Lw} plays an important role in a plume rise parameterization discussed in section 4.4.

3 Concentration calculations

The pollution concentration, c, at a given time and location may be determined by counting the number of particles in an imaginary sampling volume centered at (x,y,z):

$$c(x,y,z,t) = \frac{1}{\Delta x_s \Delta y_s \Delta z_s} \sum_{i=1}^{N} m_{pi} I \tag{17}$$

where

$$I = \begin{cases} 1 & for\ |X_i - x| < \Delta x_s/2\ and\ |Y_i - y| < \Delta y_s/2\ and\ |Z_i - z| < \Delta z_s/2 \\ 0 & otherwise \end{cases},$$

and m_{pi}, X_i, Y_i, Z_i are the mass and coordinates of the i-th particle at time t. The computed concentrations depend on the size of the sampling volume $\Delta x_s \Delta y_s \Delta z_s$ and on the number of particles N used in the computations. Confidence in this statistical estimate increases with the increase of a number of particles found in the sampling volume and can be achieved by increasing N or by expanding the sampling volume dimensions. However, an increase in N results in a growth of computer time, while an increase of Δx_s, Δy_s, or Δz_s reduces the resolution of the dispersion model. To obtain a smooth and statistically steady concentration field it is usually necessary to release a large number of particles on the order of several thousands. In a rigorous concentration calculation, the contribution of each particle mass should be weighted by the total time spent by the particle inside the sampling volume during each time step (Lamb et al., 1979). However, this requirement seems to be unnecessary in mesoscale applications where sizes of sampling volumes are usually much larger than distances traveled by the particle in one time step.

Computational efficiency of the particle model can be significantly improved by application of a kernel density estimator to calculate the concentration field from particle locations (Lorimer, 1986; Boughton et al., 1987; Yamada and Bunker, 1988; Grossmann, 1989; Uliasz, 1990b; Zannetti, 1992). The kernel method requires no imaginary sampling volumes and produces a smooth concentration distribution with a much smaller number of particles. The concentration at a given point is calculated as the sum of contributions from all particles taking into account a reflection of particles from the ground surface:

$$c(x,y,z) = \sum_{i=1}^{N} \frac{m_{pi}}{h_{xi} h_{yi} h_{zi}} \left[K(r_x, r_y, r_z) + K(r_x, r_y, r'_z) \right] \tag{18}$$

where the kernel K satisfies the condition

$$\frac{1}{h_{xi} h_{yi} h_{zi}} \int_{-\infty}^{\infty} \int_{-\infty}^{\infty} \int_{-\infty}^{\infty} K dx dy dz = 1 \tag{19}$$

and $r_x = (X_i - x)/h_{xi}$, $r_y = (Y_i - y)/h_{yi}$, $r_z = (Z_i - z)/h_{zi}$, $r'_z = (Z_i + z)/h_{zi}$. The parameters h_{xi}, h_{yi}, h_{zi} are the bandwidths which determine the degree of smoothing in each coordinate direction. The bandwidths should not be kept constant, as is done in many applications, but they should be particle dependent and change in relation to a natural length scale. Various functional forms can be used for the kernel K. The concentration estimations are not very sensitive to the functional form of the kernel. However, they depend fairly critically on the bandwidths.

Yamada and Bunker (1988) used a Gaussian kernel

$$K(r_x, r_y, r_z) = \frac{1}{(2\pi)^{3/2}} \exp\left(-\frac{r_x^2}{2}\right) \exp\left(-\frac{r_y^2}{2}\right) \exp\left(-\frac{r_z^2}{2}\right) \tag{20}$$

with particle dependent bandwidths related to σ_x, σ_y, and σ_z calculated for each particle with the aid of Taylor diffusion theory. However, this choice of the bandwidths leads to oversmoothing of concentration fields and values of these bandwidths must be limited, especially, in unstable conditions. A more computationally efficient three-dimensional parabolic kernel was discussed by Grossmann (1989):

$$K(r_x, r_y, r_z) = \frac{15}{8\pi}(1 - r^2) I, \quad I = \begin{cases} 1 & for\ r^2 = r_x^2 + r_y^2 + r_z^2 < 1 \\ 0 & otherwise \end{cases} \tag{21}$$

The application of the kernel density estimation to the Lagrangian particle model presented by Lorimer (1986) and Grossmann (1989) is a purely mathematical technique for estimating a probability density (concentration) from a sample (particle positions). It can not be interpreted physically in the context of the atmospheric dispersion problem. The bandwidths are dependent on the number of particles and are related to the standard deviations of the particle distribution. The same bandwidths are applied for all particles at a given time. The proposed method for selecting bandwidths is derived under the assumption that the concentration has a trivariate Gaussian distribution. It seriously limits applications of their approach in practice.

Since the problem of bandwidth selection for a kernel technique is not generally solved, we calculate grid-volume average concentration in most of our mesoscale applications using a very simple uniform kernel:

$$K(r_x, r_y, r_z) = \frac{1}{8} I_x I_y I_z, \quad I_\alpha = \begin{cases} 1 & for\ r_\alpha^2 < 1 \\ 0 & otherwise \end{cases}, \qquad \alpha = x, y, z \tag{22}$$

with constant bandwidths proportional to the increments of the grid used in the calculations: $h_x = \alpha \Delta x$, $h_y = \alpha \Delta y$, $h_z = \alpha \Delta z$. Typically, $\alpha = 0.5$ is selected. Larger bandwidths can be prescribed if stronger smoothing of concentration field is desired. A given particle can contribute to the concentration in several cells of the

concentration grid. For $h_x << \Delta x$, $h_y << \Delta y$, and $h_z << \Delta z$, the uniform kernel is practically equivalent to counting particles in a grid cell (17).

The importance of the technique used to calculate concentration fields from particle distributions is illustrated by an example taken from the study performed for the Shenandoah National Park in the eastern United States (Uliasz, 1993). The meteorological simulation was performed with the MESO model for idealized summer conditions when a synoptic flow interacts with sea-breeze and mountain mesoscale circulations. The modeling domain (550 × 550 × 5 km; 67 × 67 × 30 gridpoints) covers the state of Virginia and includes the Chesapeake Bay in the eastern part and the Appalachian and Blue Ridge mountains in the northwestern part of the domain. A 60-hour 3-D meteorological simulation (from 0400 LST on day 1 until 1600 LST on day 3) with the model MESO was performed for cloudless June conditions with a steady synoptic wind of 5 m/s from the northeast. In the discussed example five point emission sources with SO_2 emission rates greater than 100 g/s were taken into account. Continuous emission was simulated by releasing 240 particles per hour from the effective stack height calculated for each source. Figure 1 shows the particle distribution at 1200 LST (day 3) and 3-hour (0900-1200 LST) average surface concentration fields calculated with the aid of the uniform kernel (22) using different grid spacing ($\Delta x = \Delta y$ = 2.5, 5, 10, and 20 km, Δz = 0.1 km) and different smoothing (α = 0.5, and 1.0). Maximum surface concentrations vary more than order of magnitude: 73.3, 43.4, 38.9, 22.7, 17.1, 10.2, 7.5, and 4.8 $\mu g m^{-3}$ in the cases from A to H, respectively. Based on the discontinuities in the concentration fields in cases A, B, and C, it is obvious that the grid spacing and smoothing parameters are not adequate for the number of particles that was used in the simulation.

Unfortunately, the technique used in concentration calculations and its implication for obtained concentration values is rarely discussed in applications of particle modeling presented in literature. When designing particle simulations for given applications, it is necessary to answer a difficult question: what number of particles should be released to calculate concentrations with the required resolution, or what concentration resolution can be obtained from the released number of particles. This problem can be approached by studying sensitivity of concentration estimations in respect to the number of particles. Another approach is to use source- and receptor-oriented techniques described later in this chapter. Both techniques should provide the same values of concentration calculated at a receptor. In the discussed study, a difference between concentrations calculated at selected receptors with Δx = 10 km and α = 0.5 (case E) using source- and receptor-oriented techniques were smaller than 5 %.

Since particle simulations in mesoscale usually require a lot of computer time, it is convenient to store distributions of particles during the simulation and then to calculate the concentrations in a postprocessing module. It allows us not only to vary parameters of the kernel estimator but also to calculate different time averages of the concentration.

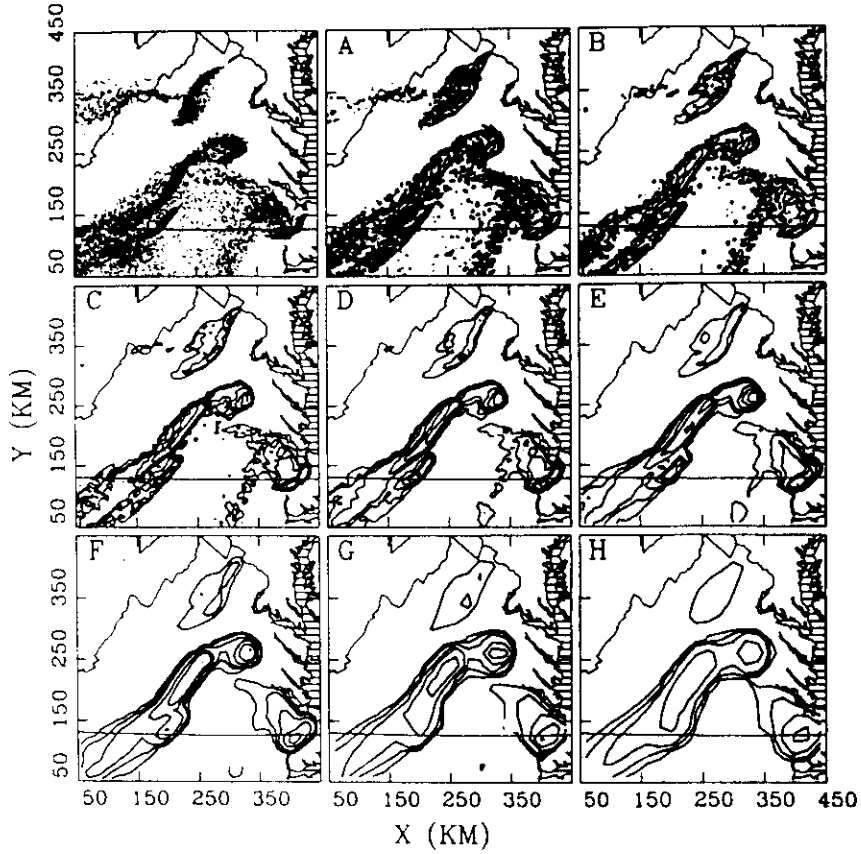

Figure 1: Distribution of particles in the Shenandoah National Park simulation and corresponding 3-hour average surface concentration fields calculated with different grid spacing and smoothing: A - Δx = 2.5 km, $h_x = 0.5\Delta x$, B - Δx = 2.5 km, $h_x = \Delta x$, C - Δx = 5 km, $h_x = 0.5\Delta x$, D - Δx = 5 km, $h_x = \Delta x$, E - Δx = 10 km, $h_x = 0.5\Delta x$, F - Δx = 10 km, $h_x = \Delta x$, G - Δx = 20 km, $h_x = 0.5\Delta x$, H - Δx = 20 km, $h_x = \Delta x$, (contours of concentration: $0.25, 0.5, 1, 2.5, 5, 10, 25, 50\ \mu g\, m^{-3}$)

4 Physical parameterizations

4.1 Chemical transformation and radiological decay

Since each particle represents a certain mass of one or more pollutants, linear chemical transformations or radiological decay can be easily included in the model. Let us consider a case of two species with concentrations, c_1 and c_2 respectively, which transformations are given by a simple chemistry mechanism (e.g., $SO_2 \rightarrow$ particulate sulfate):

$$\frac{dc_1}{dt} = -\alpha_1 c_1, \quad \frac{dc_2}{dt} = \alpha_1 c_1 - \alpha_2 c_2 \tag{23}$$

With the aid of the analytical solution of the above equation set at a given time step the mass of each particle is expressed as a sum of masses of two species $m_p = m_{p1} + m_{p2}$ which vary in time:

$$\begin{aligned} m_{p1}(t+\Delta t) &= m_{p1}(t)\exp(-\alpha_1 \Delta t) \\ m_{p2}(t+\Delta t) &= m_{p1}(t)\frac{\alpha_1}{\alpha_1-\alpha_2}[\exp(-\alpha_2\Delta t) - \exp(-\alpha_1\Delta t)] + m_{p2}(t)\exp(-\alpha_2\Delta t) \end{aligned} \tag{24}$$

The transformation coefficients, α_1 and α_2, may depend on local meteorological variables, e.g., temperature, humidity, solar radiation. A proper treatment of nonlinear chemistry may be very difficult or impossible within a Lagrangian framework (Zannetti, 1992).

4.2 Dispersion of heavy particles

Dispersion of gaseous species or fine particles with diameter $D_p \leq 1$ μm can be represented by the dispersion of the passive tracer as described in section 2. For larger particles the assumption that the turbulence characteristics of the tracer fluid or particle are similar to those of the surrounding fluid is no longer valid. The effect of gravitational forces on the mean particle motion should be included in the dispersion model by the addition of the mean particle settling velocity, v_t in equations (3). The particle attains its terminal settling velocity $v_t = T_p g$ for $t >> T_p$. The relaxation time, T_p, which is extremely short, can be determined for spherical aerosol particles as

$$T_p = \frac{D_p^2}{18\nu}\frac{\rho_p}{\rho} \tag{25}$$

where ρ_p and ρ - densities of particle and air, g - gravitational acceleration, ν - kinematic molecular viscosity. For larger particles which do not satisfy the Stokes law (Reynolds number $Re = D_p v_t/\nu > 0.1$), an empirical correction factor $f(Re)$ is required in (25).

Since the dynamic response of a heavy particle to turbulent flow is different from that of a fluid element, two additional effects must be taken into account (Yudine, 1959; Csanady, 1963):

- Inertia effect. A particle with inertia does not respond to all frequencies of atmospheric turbulence but only to those with a period much greater than its relaxation time, T_p. This selective response means that there will always be some relative motion between the particle and the surrounding air. The effect of inertia can be neglected for small particles up to 400-500 μm diameter.

- Crossing trajectories effect. As a consequence that a particle has a mean downward velocity the particle does not remain within a particular turbulent eddy but continuously drops out from the influence of eddies. The result is that a particle with a large enough terminal velocity crosses the trajectories of many eddies and loses correlation more rapidly that would a passive tracer. The crossing trajectories effect is important down to even quite small diameters.

Several authors proposed modifications to the particle dispersion model which take into account these two effects (Hunt and Nalpanis, 1985; Walklate, 1986; Walklate, 1987; Hashem and Parkin, 1991; Sawford and Guest, 1991). The inertia effect reduces the particle variance σ_{pi}^2 and increases the particle autocorrelation $R_{pi}(\Delta t)$ in comparison to the corresponding values of air velocity σ_i^2 and $R_i(\Delta t)$ while the cross trajectory effect reduces the particle autocorrelation only. It means that heavy particles may disperse faster than fluid elements if the inertia effect controls the dispersion. On the other hand, if the inertia effect is negligible, the dispersion of heavy particles is less than the dispersion of a passive tracer following fluid elements. E.g., if the inertia effect can be neglected, the autocorrelation of particle vertical velocity is expressed as

$$R_{pw}(\Delta t) = R_w(\Delta t)\exp\left(-C\frac{v_t}{\sigma_w}\right) \tag{26}$$

where C is a constant in the range 1 to 2 (Walklate, 1987). A comprehensive analysis of heavy particle dispersion was recently presented by Wang and Stock (1993).

4.3 Dry deposition

The interaction of the particle with the ground surface is parameterized following Boughton et al.(1987). Above a certain height h, the probability of particle deposition is negligible. If the particle comes below the height $z < h$, the probability that the particle is absorbed during time Δt is computed from the transition probability density given by Monin (1959)

$$\begin{aligned} P(z,\Delta t) &= \phi\left[-\frac{z - v_t\Delta t}{\sqrt{2K\Delta t}}\right] + \frac{v_d}{v_d - v_t}\exp\left(\frac{v_t z}{K}\right)\phi\left[-\frac{z - v_t\Delta t}{\sqrt{2K\Delta t}}\right] - \\ &\quad \frac{2v_d - v_t}{v_d - v_t}\exp\left[\frac{v_d z}{K} + \frac{v_d(v_d - v_t)\Delta t}{K}\right]\phi\left[-\frac{z + (2v_d - v_t)\Delta t}{\sqrt{2K\Delta t}}\right] \end{aligned} \tag{27}$$

where v_d is the deposition velocity, $\phi(x)$ is the standard Gaussian distribution, K is the eddy diffusivity, and z is the height of the particle above the ground surface. For

particles with a zero settling velocity, v_t, this equation reduces to:

$$P(z,\Delta t) = 2\left(\phi\left[-\frac{z}{\sqrt{2K\Delta t}}\right] - \exp\left[\frac{v_d(z+v_d\Delta t)}{K}\right]\phi\left[-\frac{z+2v_d\Delta t}{\sqrt{2K\Delta t}}\right]\right) \qquad (28)$$

The probability of absorption given by the above equations allows one to simulate a partial deposition of the pollutant, as well as the extreme cases of perfect reflection and perfect absorption. For a later case, the probability $P(z,\Delta t)$ is derived by taking the limit of equation (27) as $v_d \to \infty$. Two treatments of ground-level particles are possible:

- The particle which appears at $z < h$ is first moved as if no boundary were present. Then, if a random number from the uniform distribution on $[0,1]$ is less than $P(z,\Delta z)$, the particle is absorbed. Otherwise, the particle is moved as if the boundary were perfectly reflecting. This option is designed for heavy particles with a non-zero settling velocity.

- The ground-level particle is perfectly reflected from the ground surface and the particle mass is reduced by a fraction equal to the absorption probability $P(z,\Delta t)$. This option is applied for simulations with linear chemistry where each particle represents multiple species which may have different deposition velocities. For each species, the probability P is calculated separately and then a proper mass reduction is applied.

Both options can be used in the case of the passive tracer. Specification of the height h is not critical because the absorption probability falls off very rapidly as the particle moves away from the boundary.

The deposition velocities are computed with the aid of the resistance-model approach (Walcek et al., 1986):

$$v_d = (r_a + r_b + r_c)^{-1} \qquad (29)$$

The atmospheric resistance r_a is parameterized using surface layer similarity theory, the boundary resistance r_b is related to molecular transfer across a thin laminar sublayer immediately adjacent to the surface, and the surface resistance r_c is a function of land use and vegetation physiology.

This parameterization of dry deposition in the LPD model was compared against prediction of the high resolution K-theory dispersion model. A very good agreement was found for deposition fluxes calculated by the Markov-chain versions of the particle model and the K-theory model. The simplified random-walk versions of the LPD model did not perform as well. This is due to the time step used to move particles being too long for a proper treatment of the interaction of particles with the ground surface.

4.4 Buoyancy phenomena

Several modelers suggested different approaches to simulate buoyant plumes with Lagrangian particle models (Zannetti and Al-Madani, 1984 Cogan, 1985; Gaffen

et al., 1987; Shimanuki and Nomura, 1991; Van Dop, 1992; Luhar and Britter, 1992; Anfossi et al., 1993; Hurley and Physick, 1993). The most promising seems to be a model proposed by Van Dop (1992) where the additional stochastic equation describes the buoyancy evolution for each particle. However, even simpler approaches which derive an additional vertical velocity for each particle from an analytical plume rise model may still be acceptable in mesoscale applications. In our implementation, two options for treatment of buoyant plumes are considered:

- particles are released at an effective stack height, z_{eff};

- particles are released at stack top, z_s, and an additional vertical velocity, $w_p = w_b$, due to buoyancy is applied to each particle until the particle reaches the effective stack height, z_{eff}.

Plume rise calculations are based on an analytical model developed by Netterville (1990) for point emission sources. This model is based on the momentum and buoyancy conservation equations written as:

$$\frac{dM}{dt} = F - fM, \quad \frac{dF}{dt} = -N^2M - fM \qquad (30)$$

where $M = UR^2w_b$ and $F = UR^2g(T_s - T_a)/T_a$ are the downwind fluxes of vertical momentum and buoyancy, U is wind velocity, T_s and T_a are temperature of exit gases and ambient atmosphere, R is a plume radius, $f = T_{Lw}^{-1}$ is a frequency of atmospheric turbulence, and N is the Brunt-Väisälä frequency defined as $N^2 = g/T_a\, d\vartheta/dz$. The above equations may be solved analytically for atmospheric layers with constant U, N^2, and f in order to obtain height of the plume centerline above the stack, $Z(t)$, and its vertical velocity, $w_b(t)$, in each layer. The model takes into account the vertical structure of the atmosphere (vertical changes of wind, thermal stratification and turbulence) but still assumes that all meteorological fields are horizontally homogeneous in the the area where plume rise takes place. The advantage of Netterville's model is that the plume rise is terminated by the effect of ambient turbulence in neutral or unstable conditions. Vertical profiles of wind, potential temperature and Lagrangian time scale, T_{Lw}, required by this algorithm are provided by the meteorological model.

The effective stack height and/or plume vertical velocity are calculated at each time when new meteorological fields are available. Then, the buoyant vertical velocity component can be picked from the calculated table at each time step of particle motion. Optionally, it is possible to take into account the effect of the plume internal turbulence following Anfossi et al.(1993). A spectrum of z_{eff} and/or w_b profiles is calculated for a range of F values. An initial buoyancy flux is assigned randomly for each released particle from a normal distribution with mean value F_s calculated from provided stack parameters and the standard deviation equal to $F/3$. At each time step the buoyant vertical velocity component is selected for each particle from a precomputed set of values according to its initial buoyancy and current height. If the first option of plume rise calculation is selected, the particle is simply released at the height, z_{eff}, corresponding to its initial buoyancy.

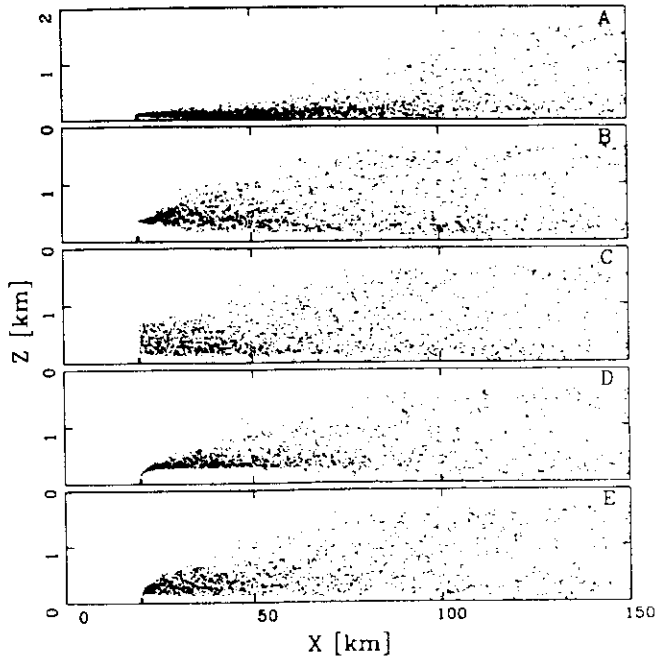

Figure 2: Comparison of plume rise parameterizations in the LPD model: A - no plume rise, B - particles released at the effective stack height, C - same as B but with initial buoyancy flux perturbations, D - additional vertical velocity due to buoyancy, E - same as D but with with initial buoyancy flux perturbations

Figure 2 illustrates the discussed variants of buoyant plume simulation with the LPD model. Meteorological profiles are obtained from a simulation of atmospheric boundary layer over homogeneous terrain. Particles are released at a rate of 720 particles per hour from a 100 m stack into a near-neutral residual layer above the stable nocturnal boundary layer. The buoyancy flux, F, for this stack is about 950 m^4/s^2

5 Evaluation of model simplifications

Computation time for the LPD model strongly depends on the number of particles to be tracked as well as on meteorological conditions and the variant of turbulent diffusion parameterization used. Only particles traveling within a specified area are considered. Figure 3 compares the computer time required by an IBM RISC 6000/550 workstation to trace 10000 particles during 1 hour using different meteorological input:

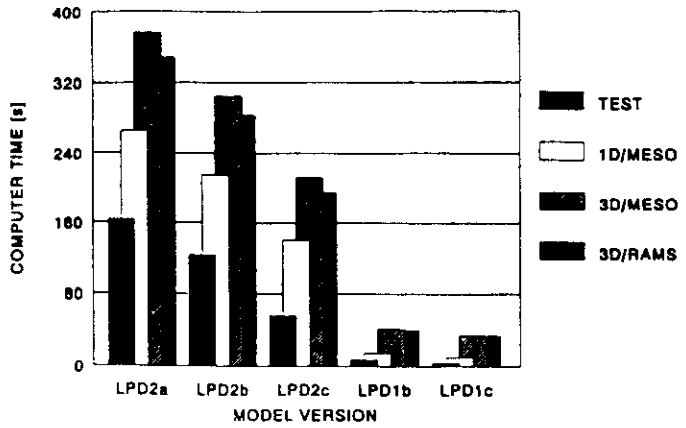

Figure 3: Computer time required by different versions of the LPD model to trace 10000 particles for 1 hour on an IBM RISC-6000/550 workstation

- a test homogeneous meteorology;
- 1-D simulation of a horizontally homogeneous boundary layer using the MESO model (60 levels up to 3 km);
- 3-D simulation of a mesoscale circulation using the MESO model (67 × 67 horizontal grid points, Δx = 6 km, 30 levels up to 5 km);
- 3-D simulation of a mesoscale circulation using the CSU RAMS (2 nested grids, particles were traced on the internal grid: 73 × 53 horizontal grid points, Δx = 12.5 km, 13 levels up to 3 km).

The particles were released randomly within a 200 × 200 × 1 km volume at the start of the test simulations. It should be pointed out that additional computer time is needed to read meteorological fields created by the meteorological model, to perform diagnostic calculations of turbulent variables, and to interpolate all variables in space for the position of each particle at each time step of the model. The interpolation may require more computer time than the advection of particles, especially, in the case of 3-D high resolution meteorological fields. The most advanced model version (LPD2a) requires interpolation of nine turbulent variables in addition to three wind components, while the simplest version (LPD1c) uses only one turbulent variable (σ_w).

The different versions of the LPD model were examined with the aid of the meteorological simulation performed for a region of complex terrain in the eastern United States (Uliasz, 1993) used already in the example presented in section 3. SO_2 concentration fields from the VA Power-Cumberland power station with an SO_2 emission rate of 489.8 gs^{-1} were simulated by each version of the LPD model. Particles

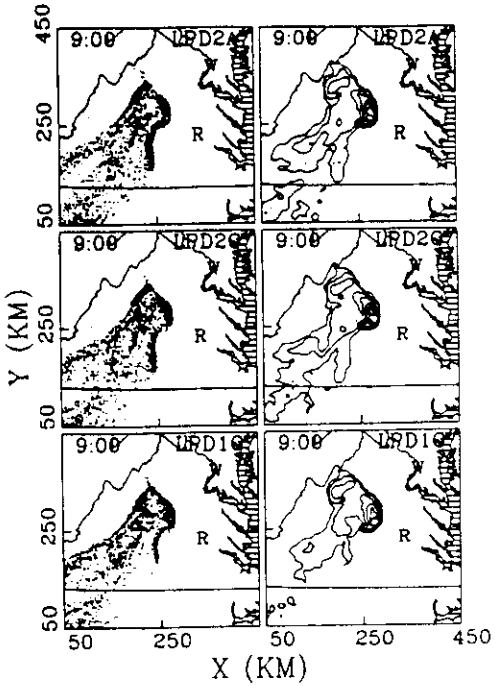

Figure 4: Particle distribution at 0000 LST (2nd day of meteorological simulation) and SO_2 surface concentration fields simulated by models LPD2a, LPD2c, and LPD1c (contours of concentration: 0.1, 0.5, 2, ..., 8, 10, 20, ... $\mu g\, m^{-3}$, W - Washington, R - Richmond, * - the receptor in Shenandoah National Park)

were released continuously at a rate of 1440 particles per hour starting at 2400 LST at the effective stack height. A time series of 3-hour average surface concentration fields were calculated from each particle simulation in $10 \times 10 \times 0.1$ km boxes with the aid of the uniform kernel (22) with $\alpha = 0.5$. Figure 4 demonstrates examples of particle distributions and surface concentrations simulated by LPD2a, LPD2c, and LPD1c models. The differences between simulations were analyzed in terms of the root mean square difference (RMS). The RMS was calculated using concentration fields from each couplet of simulations and normalized by the maximum concentration taken as a mean from these two simulations (Figure 5). The differences between all three Markov chain simulations are very small and also differences between the two random walk simulations are negligible. Differences between the most advanced model (LPD2a) and each of the random walk version are evident, however, as expressed by the RMS, they do not exceed 15% of the maximum concentrations. The RMS was also calculated for concentration fields sorted from maximum to minimum values. This operation does not significantly change the RMS which means that the random walk version

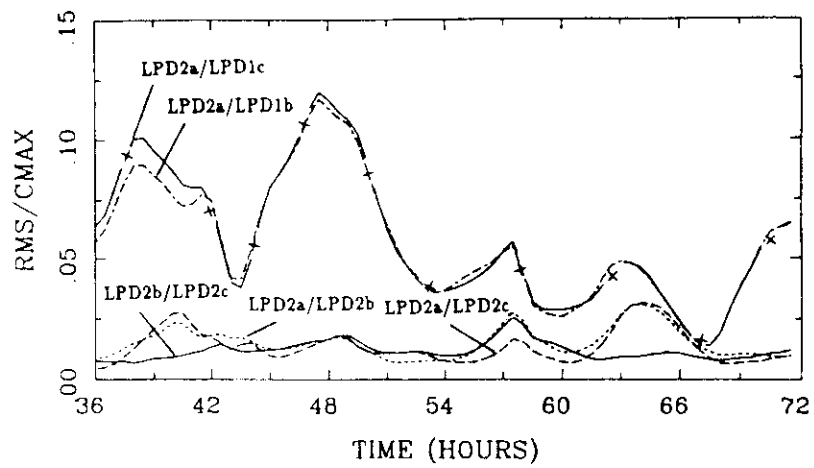

Figure 5: Time variations of difference between the surface SO_2 concentration fields predicted by different versions of the LPD model

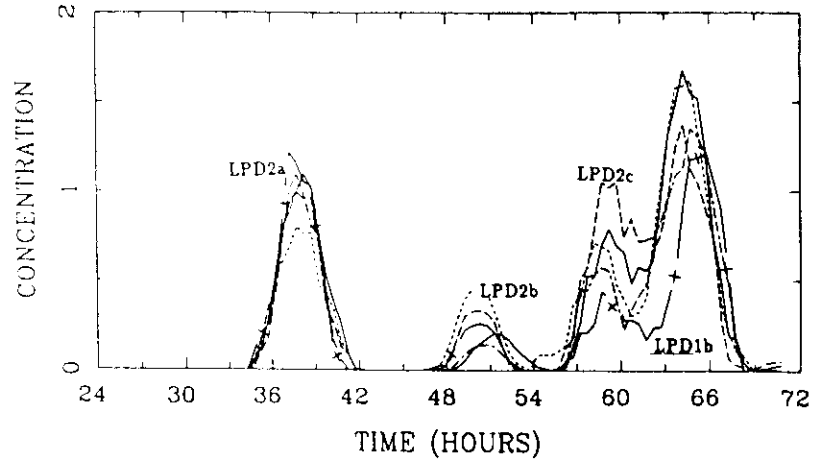

Figure 6: Time series of the surface SO_2 concentration [$\mu g\, m^{-3}$] at Shenandoah National Park predicted by different versions of the LPD model

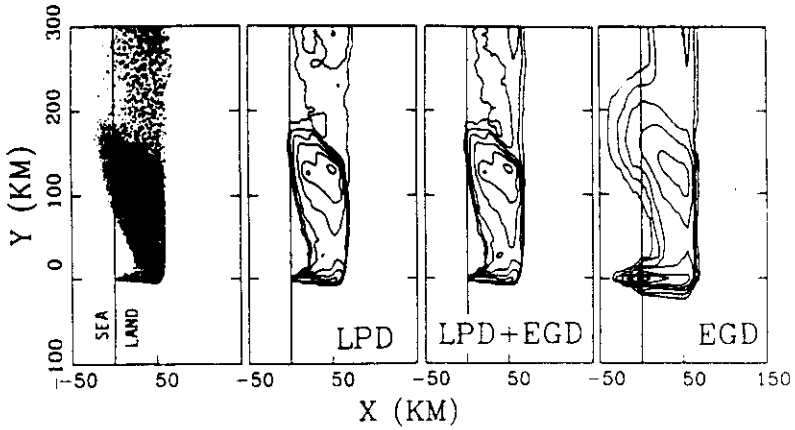

Figure 7: Particle distribution and surface concentration fields calculated by the LPD model, the hybrid dispersion model (LPD+EGD), and the EGD model at 1800 LST (logarithmic contours: -2, -1.5, -1,...)

predicts similar concentration patterns as the Markov chain version but they may under- or overestimate maximum concentrations. This conclusion is confirmed by the time series of SO_2 concentration calculated for a receptor located in Shenandoah National Park (Figure 6).

The performed simulations indicate that in mesoscale and regional applications horizontal turbulent diffusion of pollutants is not important and may be neglected. There is also no need for more refined particle models (e.g., models including wind covariances). The random walk particle models predict the same concentration pattern as the more advanced particle models, although some differences in maximum concentrations are evident. These simplified particle models are a very attractive tool for mesoscale studies since they can be an order of magnitude faster than the Markov chain models. It should be noted, however, that the random walk particle models with long time steps Δt may not be suitable for use with some physical parameterization, e.g., dry deposition or plume rise. The presented analysis of the particle models is being extended for a larger set of mesoscale dispersion simulations.

6 Hybrid dispersion modeling

Computer efficiency of the LPD model in mesoscale applications may be improved by combining this modeling technique with an Eulerian grid dispersion model based on numerical solution of diffusion equations. Due to assumption of the K-theory, the EGD model is applicable to problems whenever plume sizes are much larger then a scale of turbulent eddies in the atmosphere. On the other hand, small sources (e.g.

a single grid cell) associated with strong gradients of concentration cause significant perturbations in the numerical solution of the model equations. Therefore, the EGD model can be used for large area or volume emission sources only. The LPD model is more general and can be applied for arbitrary emission sources. However, the particle model is computationally expensive if it is necessary to track a large number of particles released from multiple sources for long distances.

It is possible to overcome these difficulties by linking the LPD and EGD models together to constitute a hybrid Lagrangian-Eulerian dispersion model (Uliasz and Pielke, 1990). After sufficiently long travel time particles are assumed to contribute to a volume emission field in the grid model and then disappear. Therefore, pollution dispersion close to point emission sources is simulated by the Lagrangian particle technique and as time increased and plume sizes are large in comparison with the grid steps, the numerical solution of the advection-diffusion equations is applied. The condition that determines when the particle contributes to the volume emission field is related to its horizontal sigma coefficients $\max(\sigma_x, \sigma_y) > \delta$ since the plume is usually resolved much faster by a vertical grid than by horizontal grid in the EGD model. The coefficients σ_x and σ_y are determined for each particle using Taylor diffusion theory by time integration of the wind velocity variances encountered during the history of the particle. The value of δ depends on the resolution of the grid model and should be assumed large enough to ensure that at least two grid cells are under the influence of each particle in the kernel calculations. The pollution concentration is determined as a sum of the concentration given by the EGD model and the concentration calculated from particles remaining in the LPD model. The simulation with the grid model can be started with a certain delay in relation to the beginning of the particle simulation when the nonzero emission field is created.

Figure 7 demonstrates an example of results from the hybrid LPD-EGD model (Uliasz and Pielke, 1991a). A two-dimensional simulation of a sea breeze over an idealized coastal area was used as meteorological input for the dispersion models. Simulations were performed for a continuous emission from a point source located at (0, 0, 0.1) km. 1000 particles per hour were released in the LPD1c model. The EGD model was run with 5 km horizontal grid spacing and 20 levels in the vertical. The number of particles was reduced by 50% (with $\delta = 1500$) in comparison with the pure particle model run at the 42-nd hour of the simulation. Concentrations were calculated from particles using the uniform kernel (22) with $\Delta x = \Delta y = 5$ km, $\Delta z = 0.1$ km, and $\alpha = 0.5$. The surface concentration fields predicted by the LPD model and the hybrid model are nearly identical while results from the pure EGD model show oversmoothing of concentrations, especially, close to the emission source.

Another possibility of hybrid modeling consists in combining two particle models with a different level of sophistication. An example of this would be the use of the Markov-chain version of the LPD model right after the release of particles from a source, and then after a prescribed travel time, the particles would be switched to the random-walk model which runs with much longer time step, Δt.

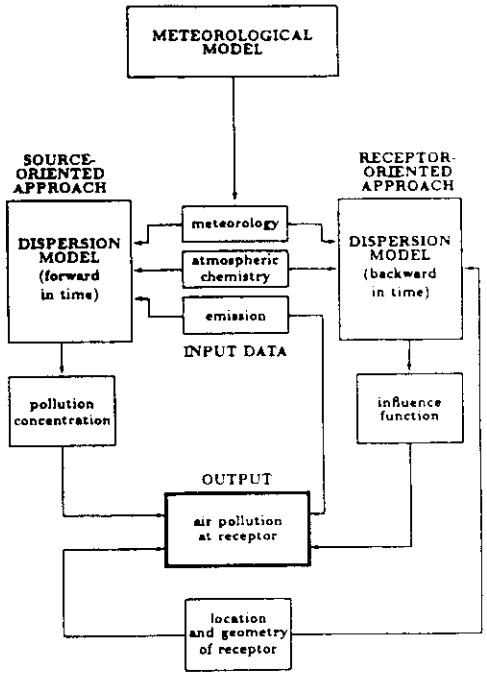

Figure 8: Source- and receptor-oriented techniques in air pollution dispersion modeling

7 Receptor-oriented dispersion modeling

The source-oriented and receptor-oriented dispersion modeling techniques can be used as complementary tools in air quality studies (Uliasz and Pielke, 1991b; Uliasz, 1993). These two alternative approaches illustrated in Figure 8 can be defined as follows:

$$\Phi[C] = \int\int R\,C\,dx\,dt = \int\int C^*\,Q\,dx\,dt \qquad (31)$$

where the source- and receptor-oriented approaches are represented by the first and second integral terms, respectively. A final goal of dispersion modeling is to calculate a certain characteristic of air pollution at a given receptor $\Phi[C]$, which can be defined, in general, as the integral of concentration, $C(\mathbf{x},t)$ over the time and space modeling domain. The receptor function, R, determines the geometry (point, area or volume) and location of the receptor and the sampling time of concentration at the receptor. Therefore, this integral expresses averaging of the concentration field over the receptor and sampling time with the weight function R.

The traditional source-oriented approach consists of solving model equations forward in time for given emission sources of pollutant $Q(\mathbf{x},t)$ to obtain a time- and

space-distributed concentration field $C(\mathbf{x},t)$. It allows us to calculate various air pollution characteristics, Φ, for any number of receptors located within the modeling domain. However, for any new emission scenario, the model solution must be in principle repeated in order to calculate Φ. This is not necessary for the LPD model if particles are tagged with their release sources.

In many practical applications when air pollution at the receptor is of primary interest, the alternate receptor-oriented modeling may be considered as a more effective approach. In this case, an influence function, $C^*(\mathbf{x},t)$ is calculated backward in time for a given receptor. The influence function, C^*, is defined by the second integral term in equation (31). It depends on meteorology, deposition, and transformations of poilutant in the atmosphere but is independent of emission sources. The air pollution at the receptor, $\Phi[C]$, may now be calculated with the aid of the influence function directly from the emission field, $Q(\mathbf{x},t)$. It should be pointed out that these calculations can be repeated for any emission field or emission scenario, Q, without additional solving of model equations. However, a new influence function must be determined for each receptor.

In the particular case when the emission field

$$Q = \sum_i e_i\,\delta(x - x_i)\,\delta(y - y_i)\,\delta(z - z_i) \qquad (32)$$

consists of multiple point sources with coordinates x_i, y_i, z_i and constant emission rates e_i, the average concentration at the receptor may be rewritten in a simple form:

$$\Phi[C] = \sum_i e_i \int C^*(x_i, y_i, z_i(t))\,dt \qquad (33)$$

where the source vertical coordinate (effective stack height), z_i, may vary in time. The above expression indicates that the time integrated influence function may be used to characterize dispersion conditions for the receptor if the emission sources are constant during the period of simulation. If the model initial and boundary conditions are taken into account, the influence function allows us to express $\Phi[C]$ as a sum of contributions from:

- local sources within the modeling domain;
- distant sources outside the modeling domain in terms of pollution flux across the model boundaries; and
- initial pollution in the modeling domain.

For a sufficiently long period of simulation the contribution from the initial concentration field is negligible.

The influence function is calculated from backward trajectories of particles in the LPD model where particles are released from the receptor during an assumed sampling time. In the case of grid dispersion models governed by partial differential equations, the influence function is obtained as a solution of the adjoint equations

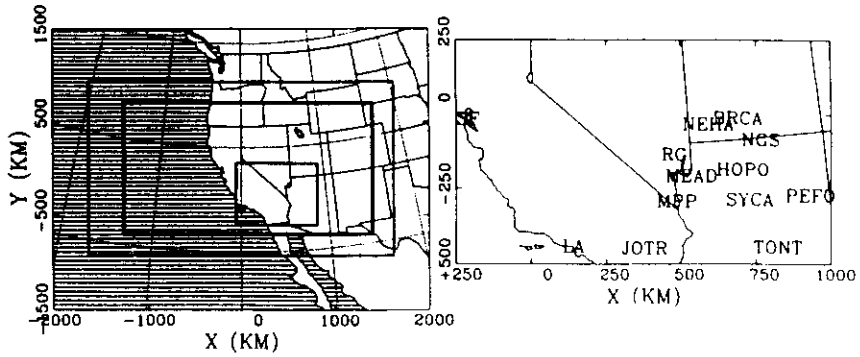

Figure 9: Modeling domain for the MOHAVE project: meteorological grids #1 and #2 - thin line rectangles, dispersion domain - thick line rectangle (left) and selected receptors and emission sources (right)

with the receptor function, R, as a source term. Applicability of the receptor-oriented option is limited to linear dispersion models. It is necessary to assume that all chemical reactions of pollutants are linear and that pollutants do not affect the atmospheric dynamics. The integral of concentration in equation (31) must also be linear, but it can be defined in an arbitrary form depending on application, particularly, it can involve concentrations of several pollutants.

8 Examples of applications

8.1 Project MOHAVE

The goal of the Measurement Of Haze And Visual Effect (MOHAVE) project is to assess the impact of the Mohave Power Project (MPP) and other potential sources of air pollution to specific Class I areas located in the desert southwest United States including the Grand Canyon National Park. The Colorado State University team is performing the daily meteorological and dispersion simulations for a year long study using a non-hydrostatic mesoscale meteorological model, the CSU RAMS coupled with the LPD model (Uliasz et al., 1993). Both the source- and receptor-oriented approaches are used. The modeling domain (Figure 9) covers the southwestern United States with its extremely complex terrain.

The design for daily dispersion simulations with an emphasis on influence function calculations using examples from the winter and summer intensive periods of the

MOHAVE project is discussed below. This very computationally intensive study is performed on two IBM RISC-6000/550 workstations, each equipped with 4 Gb external hard disks, dedicated to the project. The computations involve the four following steps: 1) meteorological simulations using the RAMS; 2) extracting and processing meteorological fields; 3) dispersion simulations using the LPD model; and 4) concentration and influence function calculations.

The daily meteorological simulations carried out with the RAMS use two interactive grids with horizontal grid increments of 50 and 12.5 km, and the number of gridpoints of $66 \times 38 \times 33$ and $74 \times 54 \times 33$, respectively. Each of the modeled days during the year is initialized with the National Meteorological Center initialization data and standard National Weather Service surface data obtained at the National Center for Atmospheric Research. These RAMS simulations do not use 4-dimensional data assimilation but update the model fields through the lateral boundaries with the conditions at the boundaries being linearly interpolated between the 12 hour observation times. For each day of the study period, 36 hours of simulation are performed with the first 12 hours being used to spin-up the atmosphere. The next 24 hour period is then used to represent the diurnal cycle of a given day.

The simplified version of the LPD model based on a fully random walking scheme and with neglected horizontal diffusion (LPDlc) was selected for this study. The computer efficiency of this particle model allows us to design a variety of dispersion simulations using daily output from the RAMS. All daily dispersion simulations are limited to the dispersion of a passive (conservative) tracer. Concentration or influence function fields are calculated from particle distributions using the uniform kernel (22) with $\alpha = 0.5\%$. The number of particles used in the study was determined empirically to be sufficient to calculate concentration using averaging boxes with sizes $50 \times 50 \times 0.2$ km. To obtain a better resolution of concentration fields, the release of a higher number of particles may be required.

Source-oriented simulations. Three series of forward in time particle simulations are currently being performed:

- Local emission sources. These simulations include three power plants: Mohave Power Project (MPP), Navajo Generating Station (NGS) and Reid Gardner (RG) power plant. Particles are released continuously from effective the stack height calculated for each power plant.

- Distant emission sources. These simulations are performed for the purpose of visualization of long range transport rather than to calculate actual concentration fields. Particles are released with a rate of 80 particles per hour continuously from $20 \times 20 \times 0.2$ km volumes located at Los Angeles, San Francisco, Phoenix and Salt Lake City. Additionally, Las Vegas is included as the closest urban area to the region of interest. A fictitious source is added in northwest Nevada in order to study the possible effect of the location of new emission sources in a so-called clean air corridor extending northwest from the Grand Canyon area. Selected particle animations from the forward in time simulations will be recorded on video tape.

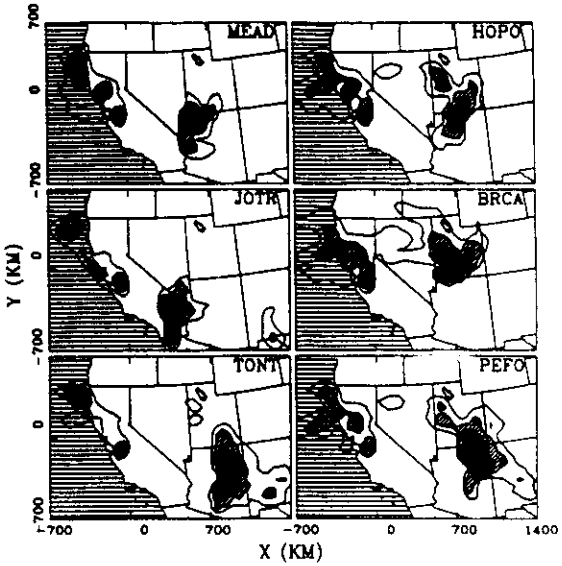

Figure 10: Time integrated influence function fields for the layer 0-500 m calculated for six selected receptors for the period January 16-31, 1992 (contours of $\log(C^*) = -12, -11.5, -11, \ldots\ s\,m^{-3}$)

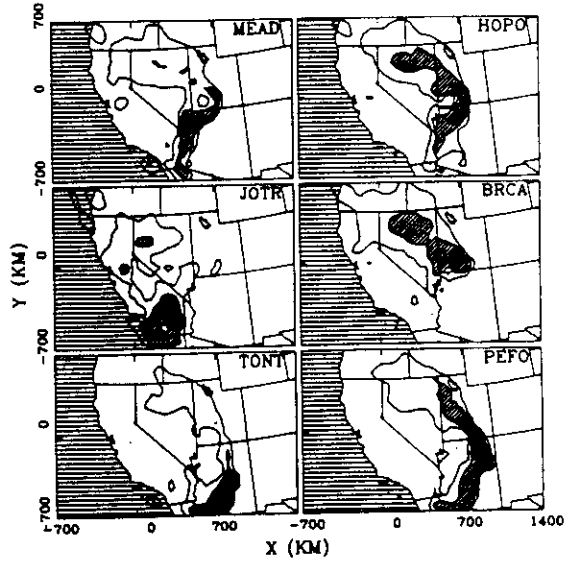

Figure 11: Same as Figure 10 but for the period July 16-31, 1992

- Tracer releases. These simulations include tracer releases from Dangling Rope, UT during the winter intensive period and El Centro and Tehachapi Pass, CA during the summer intensive period. The simulation for the MPP is being performed for the whole year.

Receptor-oriented simulations. The backward in time particle simulations are performed for nine selected receptors: Meadview (MEAD), Hopi Point (HOPO), Joshua Tree (JOTR), New Harmony (NEHA), Sycamore Canyon (SYCA), Bryce Canyon (BRCA), Tonto (TONT), Petrified Forest (PEFO), and Spirit Mountain (SPMO) (Figure 9). Particles are released during each of the 12 hour sampling periods (6am-6pm and 6pm-6am PST) from $20 \times 20 \times 0.2$ km volumes. Twelve hundred particles are released from each receptor. Particles are traced backward from receptors for five days. The simulation is terminated earlier if all particles have left the modeling domain. The influence functions are originally computed for 12 hour sampling periods and then can be combined for any longer time period.

Figures 10 and 11 present examples of the influence functions for six selected receptors calculated for two week periods during winter and summer 1992. A compact circular shape of the influence function fields in the winter cases does not necessary indicate stagnant conditions. The receptor can be still affected by pollution releases at elevations higher than 500 m as indicated by the influence functions calculated for the layer 500-1000 m. The effective stack height for NGS varies from 300 to 700 m.

The influence functions integrated over the time of simulation do not provide information about age of particles arriving to the receptor from different sources. This information as well as meteorological conditions encountered by particles between the source and receptor are important for the modeling of chemical transformations and removal processes of pollutants in the atmosphere. Therefore, particles are used to trace several meteorological variables along their trajectories: mean relative humidity, maximum relative humidity, mean temperature, and time spent within clouds. Additionally, the travel time during daylight is determined. These characteristics together with the influence functions are calculated against travel time between the source and receptor (i.e. aging time of particles) for selected point sources and a grid of area sources covering the modeling domain. Figures 12 presents an example of this type of results from the dispersion simulations for the Hopi Point receptor in the Grand Canyon National Park and three emission sources: MPP, Los Angeles (LA) and San Francisco (SF). The urban sources are represented by 100×100 km area sources.

The program of daily simulations in the MOHAVE project is strongly limited by available computer resources. In the case of dispersion simulations, the disk space is the strongest constraint. The daily meteorological simulations are performed approximately in a real time on IBM RISC workstations. The computer time required by the particle simulation is very variable since it depends on meteorological conditions. Typically, the particle simulation for nine receptors, which is run for five days backward in time, needs from 1 to 2 hours of computer time.

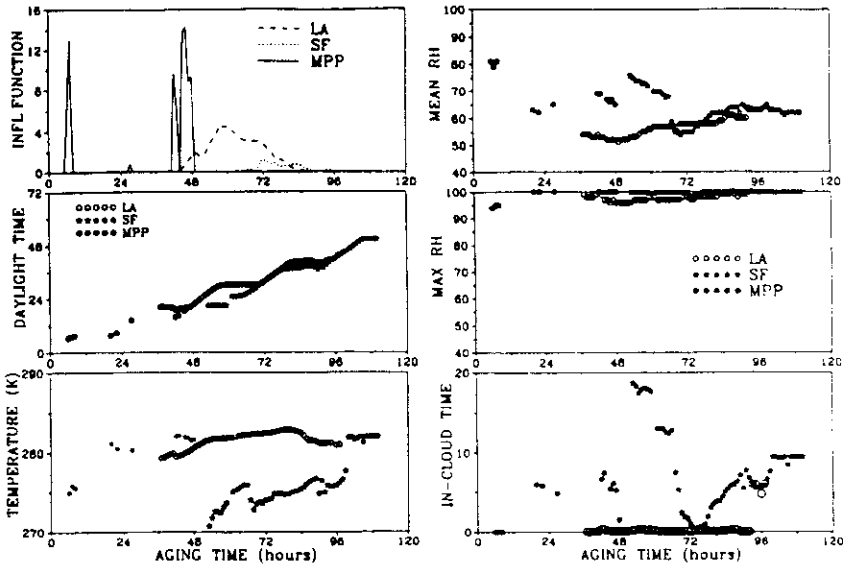

Figure 12: Distributions of influence function, daylight time, mean temperature, mean relative humidity, maximum relative humidity and in-cloud travel time with aging time of particles arriving at the Hopi Point receptor within sampling period 0600-1800 PST, February 10, 1992 and released from the MPP, Los Angeles and San Francisco sources

8.2 Black Triangle simulations

The modeling methodology developed for the MOHAVE project is being applied to the region of eastern Europe where Poland, Germany and the Czech Republic meet (Figure 13). This region called "Black Triangle" is an area with an extensive mining of hard coal and lignite, mostly by opencast methods coupled with numerous coal-fired power plants and heavy industry. There are also some national parks and large forest areas in this region. However, they have been already seriously damaged by air pollution.

The hydrostatic meteorological mesoscale model MESO together with the random walk version of the LPD model is used for preliminary simulations for the Black Triangle region. The modeling domain $300 \times 300 \times 6$ km with $31 \times 31 \times 25$ gridpoints is centered in the Sudety Mountains. One soil type (loam) is assumed in the whole modeling domain but four land-use categories are distinguished (water, urban, forest and agriculture areas). A series of 36-hours 3-D meteorological simulations for May and June 1993 was performed assuming that synoptic fields vary in time but are horizontally homogeneous within the modeling domain. Additionally, 1-D simulations are

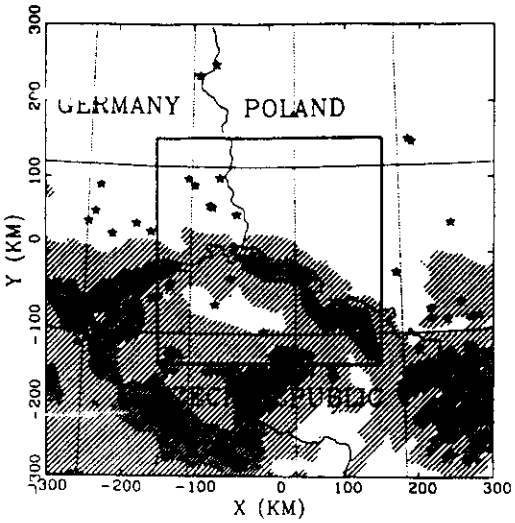

Figure 13: Black Triangle region: stars - major emission sources of SO_2, rectangles - modeling domain and receptor in the Karkonosze Mountain National Park, terrain elevation contours - 250, 500, 750, ... m

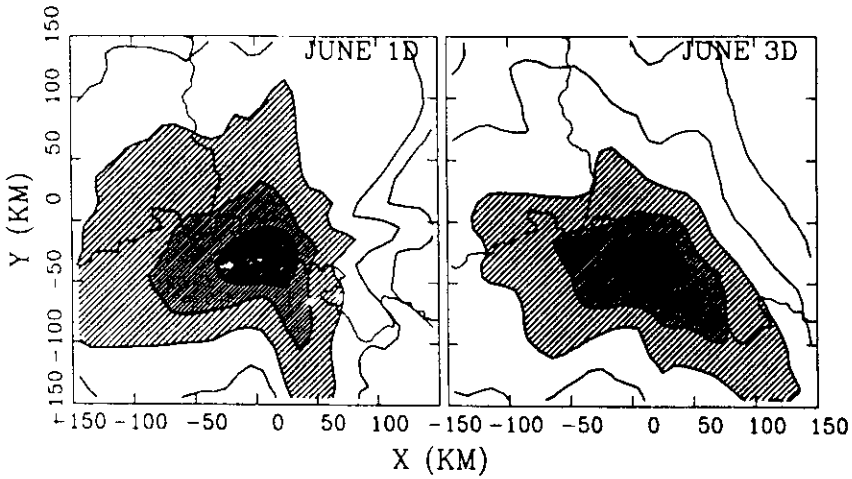

Figure 14: Time integrated influence function for June 1993 in the layer 0-500 m calculated for the Karkonosze Mountain National Park using 1-dimensional (left) and 3-dimensional (right) meteorological simulations

run for a flat and homogeneous terrain in order to study the sensitivity of pollution transport patterns in respect to the representation of terrain and surface processes parameterizations in the meteorological model. One 3-D meteorological simulation needs 2 hours of computer time on an IBM RISC-6000/550 workstation.

The LPD model is used in a receptor-oriented mode for a $20 \times 20 \times 0.2$ km receptor at the Karkonosze Mountain National Park with the highest peak in the region (Śnieżka, 1602 m). The influence functions are calculated for 12 hour sampling periods and then combined for longer periods in a similar manner to what was done in the project MOHAVE. The influence functions were computed for the whole June of 1993 using series of 1-D and 3-D meteorological simulations (Figure 14). This comparison clearly demonstrates the importance of mesoscale circulations in this mountainous region for dispersion modeling although terrain features are rather poorly resolved with the horizontal grid spacing of 10 km used in the current meteorological simulations.

The traditional source-oriented dispersion simulations would be difficult to perform at this time because of problems with the availability of reliable emission data for this region. In further research, the modeling domain will be extended in W-E direction to cover Lower and Upper Silesia in Poland, the region around Ostrava and northern Bohemia in Czech Republic, and the surrounding of Cottbus and Leipzig in east Germany. This larger domain may be called a "Sulphur Triangle" due to high emissions of SO_2. An attempt will also be made to investigate pollution dispersion patterns as represented by the influence functions with the aid of a synoptic classification (Yu and Pielke, 1986).

9 Conclusions

This chapter demonstrates the value of using state-of-the-art meteorological and Lagrangian particle dispersion models on high performance workstations in order to assess air pollution impacts over mesoscale and regional areas. The possible simplifications of the Lagrangian particle model were examined and simple physical parameterizations were implemented in order to develop an efficient tool for mesoscale applications. The source- and receptor-oriented approaches provide a different insight into regional air pollution transport. The influence functions can be very useful in application to emission control problems, especially, in defining so-called clear air corridors for the Grand Canyon National Park and other receptors in the southwestern US and assessing the emission reduction scenarios in the eastern Europe.

Acknowledgments. The author wish to thank Roger Stocker for reviewing this paper and providing valuable comments. Funding for this research was partially provided by the National Park Service through Interagency agreement #0475-4-8003 with the National Oceanic and Atmospheric Administration through agreement #CM0200 DOC-NOAA to the Cooperative Institute for Research in the Atmosphere (Project #5-31796). The physical parameterizations for the LPD model were developed under various contracts in ASTeR, Inc.

References

Andrén, A., 1990: Evaluation of turbulence closure scheme suitable for air-pollution applications. *J. Appl. Meteor.*, **29**, 224–239.

Anfossi, D., E. Ferrero, G. Brusasca, A. Marzorati, and G. Tinarelli, 1993: A simple way of computing buoyant plume rise in Lagrangian stocjastic dispersion models. *Atmos. Environ.*, **27A**, 1443–1451.

Boughton, B. A., J. M. Delaurentis, and W. E. Dunn, 1987: A stochastic model of particle dispersion in the atmosphere. *Boundary-Layer Meteor.*, **40**, 147–163.

Cogan, J. L., 1985: Monte Carlo simulation of buoyant dispersion. *Atmos. Environ.*, **19**, 867–878.

Csanady, G. T., 1963: Turbulent diffusion of heavy particles in the atmosphere. *J. Atmos. Sci.*, **20**, 201–208.

Gaffen, D. J., C. Benocci, and D. Olivari, 1987: Numerical modeling of buoyancy dominated dispersal using a Lagrangian approach. *Atmos. Environ.*, **21**, 1285–1293.

Grossmann, P. A., 1989: Kernel density estimation applied to a Lagrangian particle dispersion model. Report 10/89, Chisholm Institute of Technology, Australia.

Grubb, D. P. and R. R. Borchers, 1991: Worstations emerge as major scientific resource. *Computers in Physics* 571–573.

Hanna, S. R., 1982: Applications in air pollution modeling. In *Atmospheric Turbulence and Air Pollution Modeling*, Nieuwstadt, F. T. M. and H. Van Dop, Editors, D. Reidel Publ., Dordrecht, 275-310.

Hashem, A. and C. S. Parkin, 1991: A simplified heavy particle random-walk model for the prediction of drift from agricultural sprays. *Atmos. Environ.*, **25A**, 1609–1614.

Helfand, H. M. and J. C. Labraga, 1988: Design of a nonsingular level 2.5 second-order closure model for the prediction of atmospheric turbulence. *J. Atmos. Sci.*, **45**, 113–132.

Hunt, J. C. R. and P. Nalpanis, 1985: Saltating and suspended particles over flat and sloping surfaces. In *Proceeding of the International Workshop on the Physics of Blown Sand*, Barndorff-Nielsen, O. E., Editor, Aarhuis, Denmark, 9-36.

Hurley, P. and W. Physick, 1993: Lagrangian particle modelling of buoynat point sources: plume rise and entrapment under convective conditions. *Atmos. Environ.*, **72A**, 1579–1584.

Lamb, R. G., H. Hogo, and L. E. Reid, 1979: A Lagrangian approach to modeling air pollutant dispersion: Development and testing in the vicinity of roadway. Technical report, EPA Research Report EPA-600/4-79-023.

Legg, B. J. and M. R. Raupach, 1982: Markov-chain simulation of particle dispersion in inhomogeneous flows: the mean drift velocity induced by a gradient in Eulerian velocity variance. *Boundary-Layer Meteor.*, **24**, 3–13.

Lorimer, G. S., 1986: The kernel method for air quality modeling - I. Mathematical foundation. *Atmos. Environ.*, **20**, 1447–1452.

Luhar, A. K. and R. E. Britter, 1992: Random-walk modeling of buoyant-plume dispersion in the convective boundary layer. *Atmos. Environ.*, **26A**, 1283–1298.

Lyons, W. A., R. A. Pielke, W. R. Cotton, M. Uliasz, C. J. Tremback, R. L. Walko, and J. L. Eastman, 1993: The applications of new technologies to modeling mesoscale dispersion in coastal zones and complex terrain. In *Air pollution*, P. Zanetti, C. A. Brebia, J. E. G. and G. A. Milian, Editors, Computational Mechanics Publications, Southampton, 33-85.

Mellor, G. L. and T. Yamada, 1982: Development of a turbulence closure model for geophysical fluid problems. *Rev. Geophys. Space Phys.*, **20**, 851–875.

Monin, A. S., 1959: On the boundary condition on the earth surface for diffusing pollution. *Adv. Geophys.*, **6**, 435–436.

Netterville, D. D. J., 1990: Plume rise, entrainment and dispersion in turbulent winds. *Atmos. Environ.*, **24A**, 1061–1081.

Obukhov, A. M., 1959: Description of turbulence in terms of Lagrangian variables. *Adv. Geophys.*, **6**, 113–116.

Pielke, R. A., W. R. Cotton, R. L. Walko, C. J. Tremback, M. E. Nicholls, M. D. Moran, D. A. Wesley, T. J. Lee, and J. H. Copeland, 1992: A comprehensive meteorological modeling system - RAMS. *Meteor. Atmos. Phys.*, **49**, 69–91.

Pielke, R. A., W. A. Lyons, R. T. McNider, M. D. Moran, D. A. Moon, R. A. Stocker, R. L. Walko, and M. Uliasz, 1991: Regional and mesoscale meteorological modeling as applied to air quality studies. In *Air Pollution Modeling and Its Application VIII*, van Dop, H. and D. G. Steyn, Editors, Plenum Press, New York, 259-290.

Sawford, B. L. and F. M. Guest, 1991: Lagrangian statistical simulation of the turbulent motion of heavy particles. *Boundary-Layer Meteor.*, **54**, 147–166.

Shimanuki, A. and Y. Nomura, 1991: Numerical simulation of instantaneous images of the smoke released from a chimney. *J. Meteor. Soc. Japan*, **60**, 187–195.

Smith, F. B., 1968: Conditioned particle motion in a homogeneous turbulent field. *Atmos. Environ.*, **2**, 491–508.

Uliasz, M., 1990a: Development of the mesoscale dispersion modeling system using personal computers. Part I: Models and computer implementation. *Zeitschrift für Meteorologie*, **40**, 104–114.

Uliasz, M., 1990b: Development of the mesoscale dispersion modeling system using personal computers. Part II: Numerical simulations. *Zeitschrift für Meteorologie*, **40**, 285–298.

Uliasz, M., 1993: The atmospheric mesoscale dispersion modeling system. *J. Appl. Meteor*, **32**, 139–149.

Uliasz, M. and R. Pielke, 1990: Receptor-oriented Lagrangian-Eulerian model of mesoscale air pollution dispersion. In *Computer Techniques in Environmental Studies III*, Zanetti, P., Editor, Computational Mechanics Publications, Southampton and Springer-Verlag, Berlin, 57-68.

Uliasz, M. and R. Pielke, 1991a: Lagrangian-Eulerian dispersion modeling system for real-time mesoscale applications. In *Third Topical Meeting on Emergency Preparedness and Response*, Chicago, Illinois, April 16-19, 1991, 95-98.

Uliasz, M. and R. A. Pielke, 1991b: Application of the receptor oriented approach in mesoscale dispersion modeling. In *Air Pollution Modeling and Its Application VIII*, van Dop, H. and D. G. Steyn, Editors, Plenum Press, New York, 399-408.

Uliasz, M. and R. A. Pielke, 1993: Implementation of Lagrangian particle dispersion model for mesoscale and regional air quality studies. In *Air pollution*, P. Zanetti, C. A. Brebia, J. E. G. and G. A. Milian, Editors, Computational Mechanics Publications, Southampton, 157-164.

Uliasz, M., R. A. Stocker, and R. A. Pielke, 1993: Numerical modeling of atmospheric dispersion during the MOHAVE field study. In *Air pollution*, P. Zanetti, C. A. Brebia, J. E. G. and G. A. Milian, Editors, Computational Mechanics Publications, Southampton, 208-216.

Van Dop, H., 1992: Buoyant plume rise in a lagrangian framework. *Atmos. Environ.*, **26A**, 1335–1346.

Walcek, C. J., R. A. Brost, J. S. Chang, and M. L. Wesely, 1986: SO_2, sulfate and HNO_3 deposition velocities using regional land use and meteorological data. *Atmos. Environ.*, **20**, 949–964.

Walklate, P. J., 1986: A Markov-chain particle dispersion model beased on air flow data: extension to large water droplets. *Boundary-Layer Meteor.*, **37**, 313–318.

Walklate, P. J., 1987: A random-walk model for dispersion of heavy particles in turbulent air flow. *Boundary-Layer Meteor.*, **39**, 175–190.

Wang, L.-P. and D. E. Stock, 1993: Dispersion of heavy particles by turbulent motion. *J. Atmos. Sci.*, **50**, 1897–1913.

Yamada, T. and S. Bunker, 1988: Development of a nested grid, second moment turbulence closure model and application to the 1982 ASCOT Brush Creek data simulation. *J. Appl. Meteor.*, **27**, 567–578.

Yu, C.-H. and R. A. Pielke, 1986: Mesoscale air quality under stagnant synoptic cold season conditions in the lake powell area. *Atmos. Environ.*, **20**, 1751–1762.

Yudine, M. I., 1959: Physical consideration on heavy-particle diffusion. *Adv. Geophys.*, **6**, 185–191.

Zannetti, P., 1986: Monte-Carlo simulation of auto- and cross-correlated turbulent velocity fluctuations (MC-LAGPAR II model). *Environmental Software*, **1**, 26–30.

Zannetti, P., 1992: Particle modeling and its application for simulating air pollution phenomena. In *Environmental Modelling*, Melli, P. and P. Zannetti, Editors, Computational Mechanics Publications and Elsevier Applied Science, 211-241.

Zannetti, P. and N. Al-Madani, 1984: Simulation of transformation, buoynacy and removal processes by Lagrangian particle methods. In *Proc. of the 14th International Technical Meeting on Air Pollution Modeling and Its Application*, de Wispelaere, C., Editor, Plenum Press, New York, 733-744.